Int. J. Multiphase Flow Vol. 11, No. 4, pp. 535–551, 1985
Printed in the U.S.A.

0301-9322/85 $3.00 + .00
Pergamon/Elsevier

THE MEASUREMENT OF BUBBLE FLOWS IN FLUIDIZED BEDS BY ELECTRICAL PROBE

D. J. GUNN and H. H. AL-DOORI
Department of Chemical Engineering, University College of Swansea, Singleton Park, Swansea SA2 8PP, United Kingdom

(*Received* 20 *March* 1984; *in revised form* 10 *October* 1984)

Abstract—Measurements of bubble velocities, dimensions and flow rates in a two-dimensional fluidized bed by a dual electrical capacitive probe are compared with measurements from cine photography; the cine photographs and electric measurements were taken at the same point in a fluidized bed and at the same time. It was found that both sets of measurements were in agreement only when the conditions of electrical measurement were arranged to exclude spurious signals, while still retaining sensitivity, and when the theory of measurement included the effects of bubble retardation and distortion, and allowed for the stochastic incidence between the bubble front and the probes.

INTRODUCTION

The formation and distribution of bubbles in gas-fluidized beds is the predominant influence in gas phase mixing while the circulation patterns of solid particles are a result of bubble distribution and flow. Several investigators have measured the velocities of single bubbles and found reasonable agreement with the Davies & Taylor (1950) equation. However, the measurements show some scatter and different values of the constant of proportionality between the bubble velocity and the square root of the bubble diameter have been reported.

The measurement of bubble velocities and flows when there are many bubbles is much more difficult because the trajectories of individual bubbles cannot usually be identified. There are two basic experimental methods. If the passage of a bubble in a fluidized bed interrupts a beam of gamma or x rays there is a consequent reduction of the absorption of the beam by the bed because of the low solids content of the bubble. If the signal is processed by an image intensifier, images of individual bubbles may be recorded and measured. The method is limited by the condition that the probability of two bubbles in line intersecting the beam should be small because the images of individual bubbles cannot be identified in a crowd of bubbles.

The second method is based upon the development of probes that are inserted in the bed and respond to capacitance, conductivity, inductance or other local property of the bed that is changed in a major way when the normal probe environment of dense phase solid is perturbed by the passage of a bubble. Single conductivity probes have been used by Goldschmidt & LeGoff (1967) in a bed of conducting particles and by Neal & Bankoff (1963). Single capacitance probes have been used by Bakker (1958), Morse & Ballou (1951), Lockett & Harrison (1967) and Geldart & Kelsey (1972). Lockett & Harrison, and Geldart & Kelsey photographed bubbles striking the probe and the latter workers recorded some flattening and splitting of bubbles by the probe.

Information that may be obtained from a single probe is limited, and therefore several workers have used dual probes. Lanneau (1960) used two plate capacitance probes separated by 75 mm with the electrical output registered on an oscillograph; the vertical separation of 75 mm permitted extensive bubble deformation and splitting between probes. Yasui & Johansen (1958) employed dual optical probes separated by a vertical distance of 25 mm in a similar manner. Park *et al.* (1969) used a dual electro-resistivity probe to study local conditions of bubbling in a fluidized bed of conductive coke particles. The probes were separated by a vertical distance of 9.5 mm and the wall electrodes, common to both probes,

consisted of silver shims attached to the inside wall of the column. Signals of amplitude >0.5 V were taken to represent bubbles, and those below this level were taken as noise. Some 10% to 25% of the signals recorded on one channel did not show corresponding signals on the other.

Werther & Molerus (1973) used a dual miniature capacitance probe. A needle 0.4 mm in diameter and 2.8 mm long formed one pole of the condenser and the surrounding metal tube, 1.1 mm in diameter, formed the other pole. Analogue cross-correlation of the signals from the two channels was used to obtain the mean delay time between poles. Werther (1974) also used twin capacitance probes at the same horizontal level to study horizontal dimensions of bubbles.

Probes having more than two sensing elements have been employed. Thus Whitehead & Young (1967) used a grid of 196 light probes recorded on cine film to study bubbles in large diameter fluidized beds. Burgess & Calderbank (1975) used a compound resistivity probe containing five elements coupled to an on-line computer; only bubbles symmetrically placed with respect to the probes were recorded, and because of the requirements of symmetry only a small fraction of bubbles that contacted the probes were recorded. An optical probe based upon similar concepts was examined by Calderbank & Pereira (1977). A compound probe with three symmetry elements has been used by Werther (1977).

Rowe & Masson (1980) simultaneously observed bubbles in a fluidized bed by probe and by x rays using an optical probe with signal discrimination by the method of Werther (1973) who assumed that bubbles give rise to triangular pulses superimposed upon noise, and set discrimination voltages to select only such pulses. They comment on their comparison (p. 1446 top) "but total lack of correlation is disturbing and not easy to understand." In a second paper (Rowe & Masson 1981) they used a different probe and commented on their comparison of bubble rise velocities. "The results are shown in Fig. 17 and indicate a weak correlation between the two methods of measurement contrary to our earlier report." They comment further (p. 184) "Apart from the fact that probes disturb the bubbles they intend to measure, some of the assumptions made in interpreting the signal line trace appear questionable."

The questions raised by Rowe & Masson are important; it is a major criticism that there has been no independent method of discriminating between bubble signals and superimposed noise. Instead discriminating circuits have been employed to reject noise by the setting of a threshold voltage that has not been independently determined by choosing the coincidence of bubble and electrical signal. There are two other major criticisms. It has always been assumed in interpreting signals that the surface of the bubble is horizontal at the point of impact with the probe, even though deformation has been observed. The third criticism is that the effect of the probe upon bubble properties has not been independently assessed. Probes have been made small to minimise interferences with bubble flows, but although the head of the probe may be small, a structure of substantial strength is required to maintain the position of the probe against buffeting so that a short length of slender probe is connected to a substantial arrangement to maintain the probe in position and to carry the probe cables.

The dual miniature probe, vertically aligned, appears to be the most promising instrument for the measurement of bubble flows in three-dimensional beds, but calibration is required. In this paper, we describe the construction of a dual miniature probe.

A two-dimensional fluidized bed was chosen for the calibration since multibubble flows could be accurately recorded; the probe was placed in the bed and simultaneous electrical and optical recordings were made of several sequences of bubble interactions with the probe. There are some differences between two and three-dimensional fluidized beds that have been measured in detail by Rowe & Everett (1972). The principal differences they found were a higher minimum velocity for fluidisation that they attributed to the greater flow of gases in

regions of high porosity near the wall, and differences in the development of bubble size and number with height in the bed, that may be attributed to the reduced opportunities for bubble coalescence in two-dimensional compared with three-dimensional fluidized beds. Neither of these factors is a difficulty in the use of the two-dimensional bed for calibration, because the procedure is concerned with the simultaneous observation of the local incidence between bubble and probe, and not with the overall pattern of bubble flow.

The correlation of optical and electrical records is described, and physical deformations of the bubble by the probe have been measured. A statistical theory of probe operation based upon the observations, is given and verified in experiment. The application of the probe to the study of bubble flows in a bed of diameter 0.3 m is described in a companion paper.

EXPERIMENTAL ARRANGEMENT

The capacitance probes

Two identical capacitance probes were used. Each probe element was made by flattening the end of a carrier tube 4 mm in diameter and 75 mm long to form one pole of the condenser. The other pole was made from a rectangular steel plate 10 mm long, 0.5 mm thick and 3 mm in width. The gap between the poles was filled with solid organic dielectric to give an overall diameter of 4 mm. The probe was fitted into a steel carrier tube 6 mm o.d., 2 m long, that protected the probe cables and provided suitable rigidity when immersed in a bubbling fluidized bed. A diagram of the probe is shown as figure 1.

Two probes were used in almost vertical alignment separated by a vertical distance that was finally arranged at 11 mm after preliminary experiments.

Each probe was part of an oscillatory bridge circuit resonating at 10 MHz, the output of which was fed to a dc amplifier with both bridge and amplifier at the top of the carrier tube.

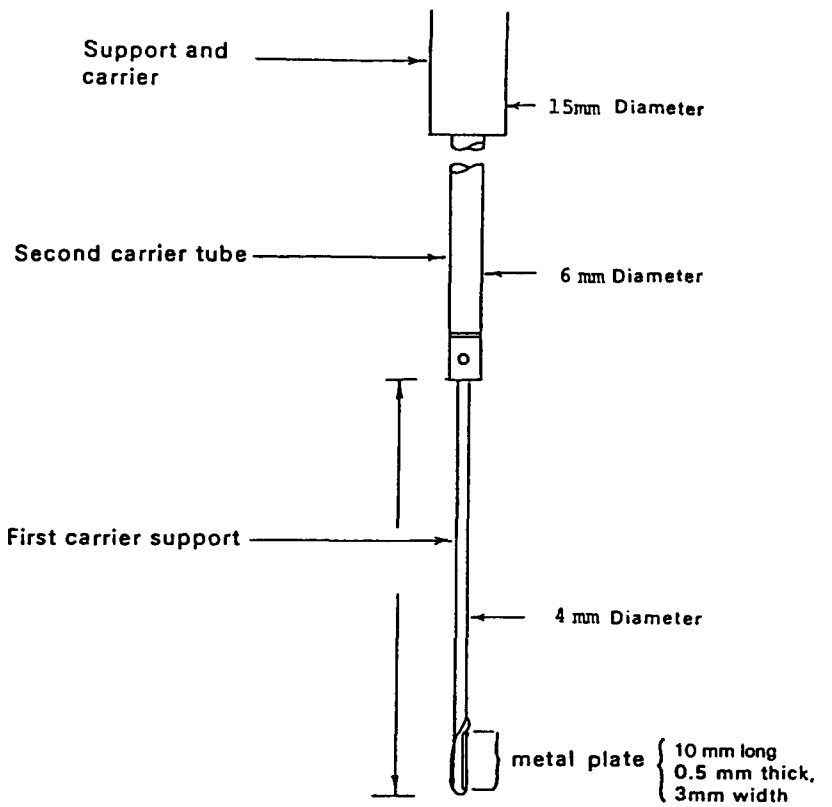

Figure 1. Diagram of probe arrangement showing supports.

A constant supply of 10 MHz frequency was achieved by using a crystal-controlled frequency generator.

Before operation the circuits were tuned to resonate at 10 MHz by altering the inductance of the resonating coil and adjusting the capacitance of a variactor diode. A voltmeter was connected to the output of this bridge amplifier to give an immediate check on the stability of the resonating circuit and the sensitivity of the probe to changes in bed porosity in the vicinity of the probe. The amplitude of the signals varied between 0 to -2 V. A discriminating voltage that could be selected from one of nine preset levels was applied to reject signals smaller than gate voltage, and signals admitted by the gates were shaped to give rectangular pulses of amplitude -2.5 V. Figure 2 shows the relationship of the input to output signals for two chosen gating levels as seen on a double beam storage oscilloscope.

Recording of the signals

Sharp pulses of 5 μs duration were induced from the leading edge of each pulse and the trailing edge of the pulse from the leading probe and the two time intervals, illustrated in figure 3, were recorded by two six digit timer counters.

It may be seen from figure 3 that there are two feasible sequences of pulses to the counters. In the first sequence the leading edge of a bubble signal from the first probe is followed by the leading edge of a bubble signal from the second probe and terminated by the trailing edge of the bubble signal from the first probe. In the second sequence the leading edge of a bubble signal from the first probe is followed by the trailing edge of the bubble

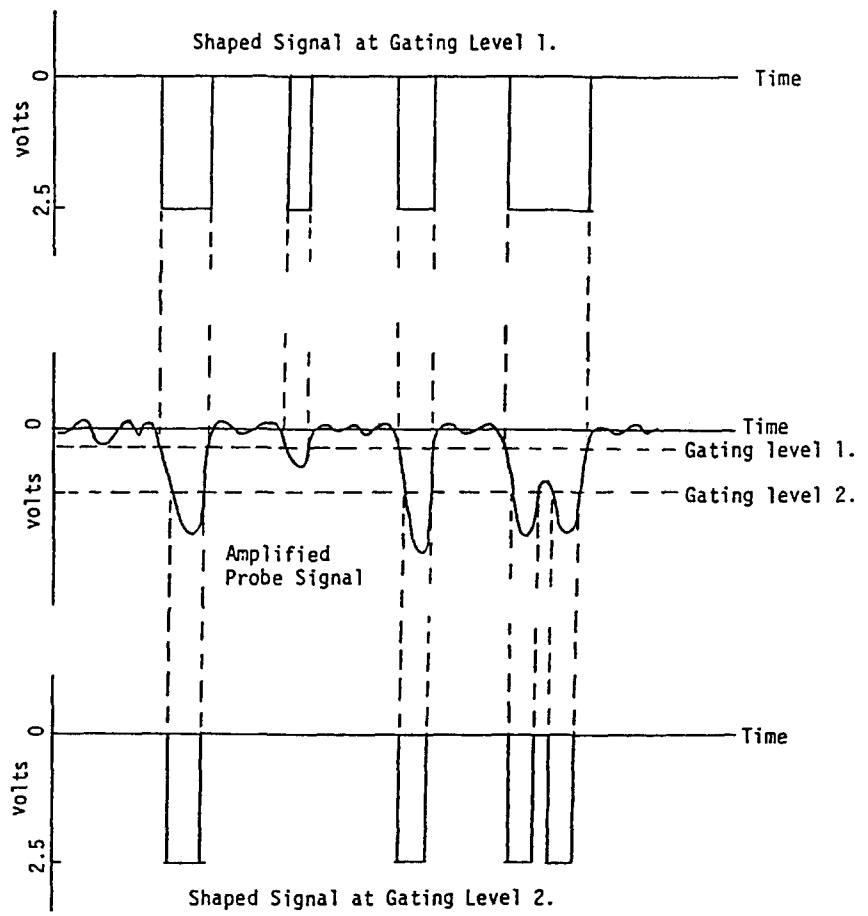

Figure 2. Illustration of probe amplifier output showing the shaping of signals.

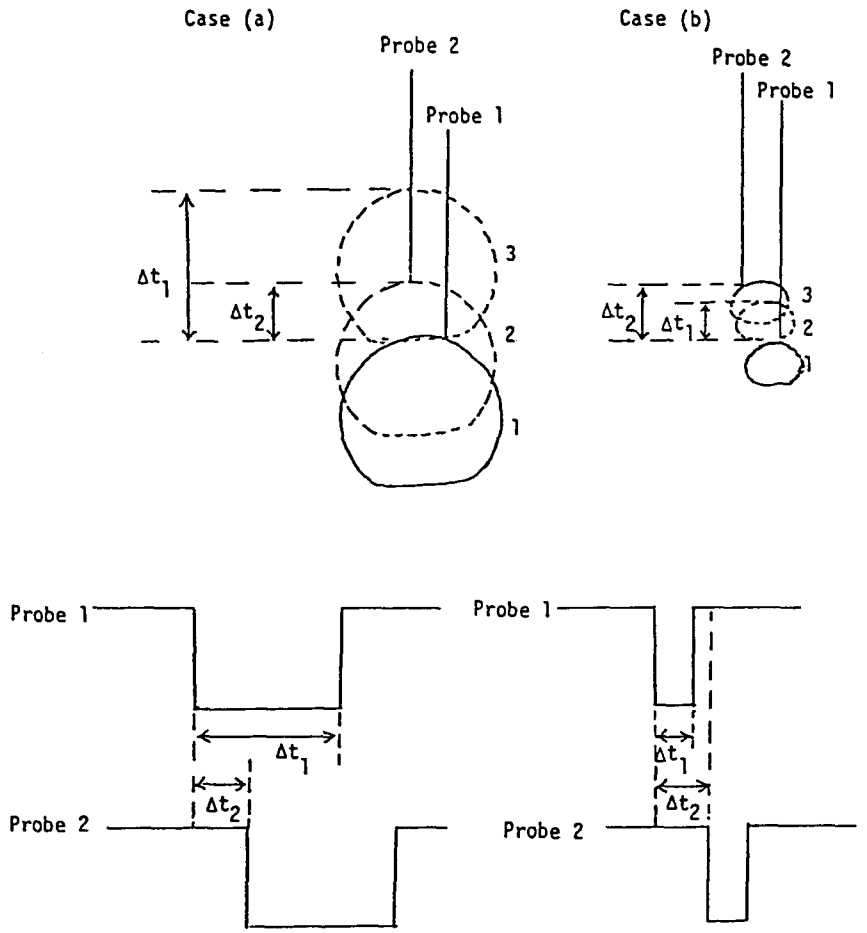

Figure 3. Illustration of probe position with respect to the bubble and the allowable sequences (a) and (b).

signal from the first probe, and the sequence is terminated by the leading edge of the bubble signal from the second probe. Only these feasible sequences were accepted for recording.

The timer counters provided the time intervals as B C D coded signals that were recorded either by a paper tape punch, or asynchronously on an industry compatible magnetic tape. The paper tape punch was used to verify the operation of the system, but the tape recorder was used in the bubble experiments; the maximum recording speed was 1738 events per second.

Before recording an experiment the operation of the timer counters and recorders was checked by feeding a known pulse chain to the input of the pulse shaper-gate unit.

Optical studies of the probe

The probes were studied by photographing bubbles passing the probes in a thin transparent fluidized bed and comparing the cine-photographic record with the simultaneous electric output of the probes. The same region of the fluidized bed was photographed under the same conditions of bubble flow but without the probes in position so that the effect of the probes upon bubble flow could be determined by comparison of the photographic records of bubble flow with and without the probes in position.

The fluidized bed was constructed from two toughened glass sheets 1.82m high, 1.15m wide and 12.5 mm thick, held in an aluminum alloy frame so that the thickness of the fluidized bed was 15 mm. Air was metered by a set of rotameters and distributed across the

width of the bed by a hollow bar at the base of the bed containing 45 evenly spaced holes each 1.5 mm in diameter. Glass ballotini of diameter 500 μm (U_{mf} = 0.30 m/s) were loaded into the bed to a height of 0.8 m above the distributor.

The dual miniature capacitance probes were fixed vertically in the fluidized bed at a height of 0.40 m above the distributor in the centre of the bed and supported by a horizontal nylon bar that fitted firmly between the glass plates above the surface of the bed, and was drilled with several evenly spaced holes to allow gas to pass. The bed was allowed to fluidize at a velocity that was maintained constant in the experiments at 1.7 times the minimum fluidization velocity.

Photographic procedure

A Bolex 16 mm cine camera was used for filming the two-dimensional bed, backlighted by 2000 W, at a nominal speed of 24 frames per second. A frame counter and the timer counters were included in the view of the camera.

After checking the operation of the probe, a discriminator gate level was selected, filming was started and, after 100 frames, a magnetic recording of 3000 frames was made.

The simultaneous filming and recording was repeated six times at different voltage gate levels keeping other factors unchanged. A further film was taken when the bed was fluidized at the same gas velocity, but without the probes. The former position of the tip of the probe was marked on the fluidized bed before taking the last film.

The timer counters in the view of the camera were used to determine the number of bubbles not detected by the probe system and helped to outline some of the reasons behind the failure of the system to record some bubbles at various gate levels.

ANALYSIS OF THE PHOTOGRAPHIC RECORD

Simulation of the probe recording

The cine film was projected onto the clear screen of a Benson–Lehner digitizer, and the tip of the lower probe and the vertical axis of the probe were marked on the screen. The film was advanced frame by frame as a bubble approached the tip of the probe, and when the bubble was nearest to the tip of the probe, a crosswise cursor was aligned at the intersection of the bubble and the vertical axis of the probe, the record button was pressed and the X and Y coordinates of the intersected point were punched into an 80 column card. The film was advanced one frame and the coordinates of the intersection of the vertical axis of the probe

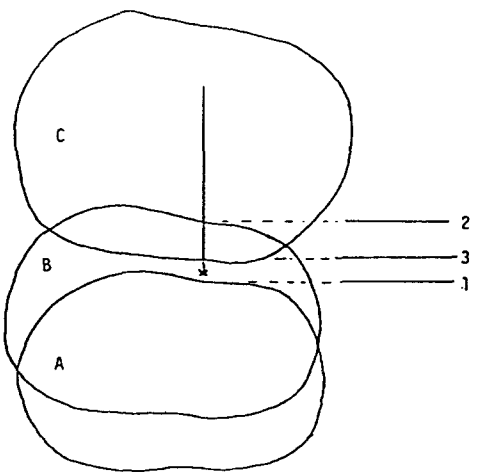

Figure 4. Optical simulation of bubble analysis.

and the bubble surface were punched into the same card. The film was then advanced frame by frame until the lower surface of the bubble was nearest to the mark, when the coordinates of the point of intersection of the vertical axis of the probe with the lower surface of the bubble were also punched out. The record for each bubble was completed by adding the number of frames between the first registration of the upper surface of the bubble and the registration of the lower surface, and an identification number for the bubble; but if the bubble was not recorded by the timer counters a further number was added so that the counting efficiency of the probe could be analysed.

When the last bubble in the filmed sequence had been analysed the total number of frames analysed was punched into the record. The three positions marked in the recorded sequence are illustrated by figure 4.

For each bubble the time interval $\Delta t_1 = \Delta t[N + (Y1 - Y3)/(Y2 - Y1)]$, the time interval between the leading and closing surfaces of the bubble striking the first probe, and $\Delta t_2 = \Delta t \cdot h/(Y2 - Y1)$, the time interval between the bubble striking the leading and following probe, were calculated; where Δt was the time interval between frames, $Y1$, $Y2$ and $Y3$ were the y coordinates of the three bubble positions illustrated in figure 4, h was the vertical distance between the upper and lower probe and N was the number of frames recorded between the upper and lower surfaces of the bubble.

The simultaneous filming and recording was repeated six times at different voltage gate levels keeping other factors unchanged. A further film was taken when the bed was fluidized at the same gas velocity, but without the probes. The former position of the tip of the probe was marked on the fluidized bed before taking the last film.

The timer counters in the view of the camera were used to determine the number of bubbles not detected by the probe system and helped to outline some of the reasons behind the failure of the system to record some bubbles at various gate levels.

Consider a bubble rising onto the probe. The interface velocity U_s is related to the time interval Δt_2 by

$$U_s = h/\Delta t_2 \qquad [1]$$

so that if δa is the effective detecting area of the probe, the incremental bubble volume δQ_B passing through the area δa is

$$\delta Q_B = \delta a \, P_L, \qquad [2]$$

where P_L is the penetration length of the probe through the bubble. The penetration length is related to U_s by

$$P_L = U_s \, \Delta t_1. \qquad [3]$$

Thus if N bubbles are recorded in a time Δt, the volumetric bubble flowrate may be found by summation of [2],

$$Q_B = \sum_{i=1}^{N} \delta Q_B/(\delta a \Delta t) = \frac{h}{\Delta t} \sum_{i=1}^{N} \left(\frac{\Delta t_1}{\Delta t_2}\right)_i. \qquad [4]$$

An additional photographic analysis of bubble flow

While the simulation method corresponds to the ideal action of a probe, a different though complementary view may be obtained by measuring the motion of complete bubbles. For each bubble the coordinates of four points that marked the intersection of the major and minor axes of an equivalent ellipse were located and automatically punched into an 80

column card. Another set of four points best fitting an ellipse was located for the same bubbles on the next 16 mm frame, and the coordinates punched into a second card. From these readings the coordinates of the centroid of the bubble were calculated as well as the major and minor axes. The velocity of the centroid of the bubble and the direction of the velocity vector were calculated from the successive frames.

If AB and CD are the major and minor axes of the ellipse, the equivalent bubble diameter is given by

$$D_e = \sqrt{(\mathrm{AB} \times \mathrm{CD})} \qquad [5]$$

and the bubble volume is $\pi/4\ D_e^2 b$ where b is the spacing between the plates.

The volumetric bubble flow per unit area over a period ΔT is

$$Q_{BC} = \frac{\pi}{4\Delta T} \sum_{i=1}^{N} \left(\frac{D_e^2 b}{Db} \right), \qquad [6]$$

where D is the average horizontal extent of the bubbles.

The mean equivalent diameter is

$$\overline{D}_e = \sqrt{\left(\sum_{i=1}^{N} (D_e^2)_i / N \right)}. \qquad [7]$$

The analysis was carried out for the same bubble sequences analysed by the simulation method.

The influence of the probe upon bubble shape and direction

The orientation of bubbles near the probe was examined by analysing the records of individual bubbles. Consider the ellipse best representing a bubble as shown in figure 5; the indicated points 1, 2, 3 and 4 are those registered on the data card as the points of intersection between perimeter and axes. The ratios d_2/d_1 and c_2/c_1 as shown in the figure were calculated for each bubble passing through the probe. The ratio d_2/d_1 will be equal to the ratio of major to minor axes when the major axis is horizontal, and to the ratio of minor to major axes when the minor axis is horizontal. The mean values for both d_2/d_1 and c_2/c_1 are shown in table 1. The average aspect ratio d_2/d_1 and the average ratio of the major and minor axes of the bubbles both varied between 1.22 and 1.29 to show that on average the major axis of the ellipse representing the bubble was horizontal, and therefore there was a preferential foreshortening of the bubble in the direction of rise. It is also evident that the

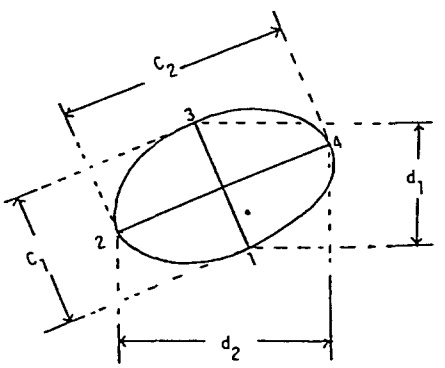

Figure 5. Elliptical representation of bubble.

Table 1. Mean values of the aspect ratio d_2/d_1 and the axis ratio c_2/c_1 of bubbles (figure 5)

Film no.	No. of bubbles	d_2/d_1	c_2/c_1	State of bed
1	140	1.22	1.24	probe present
2	149	1.22	1.22	probe present
3	144	1.29	1.29	probe present
4	150	1.28	1.28	probe present
5	135	1.24	1.25	probe present
6	125	1.27	1.27	probe present
7	149	1.22	1.23	no probe

presence or absence of the probe had no apparent effect either upon the overall shape of the bubble, or upon the preferred orientation during rise.

For the perfect ellipse the average penetration length when the major axis is horizontal is

$$\overline{P}_L = \frac{1}{c_2}\int_{-c_2/2}^{c_2/2} y\,dx = \frac{\pi}{4}\frac{c_1 c_2}{c_2} \qquad [8]$$

and since $\overline{D}_e = \sqrt{c_1 c_2}$,

$$\frac{\overline{P}_L}{\overline{D}_e} = \frac{\pi}{4}\sqrt{\frac{c_1}{c_2}}. \qquad [9]$$

Thus when the ratio of major to minor axes is 1.23, the ratio of $\overline{P}_L/\overline{D}_e$ from this equation is 0.708.

The representation of bubbles by equivalent ellipses provided the means of determining the angle at which a bubble approaches the probe because the centroid of the bubble was located at frame before and the frame after the probe met the leading surface of the bubble. From the bubble coordinates and the known time interval between frames the horizontal and vertical components of the centroid velocity vector were found and the angle of approach γ defined as $\tan^{-1}$ (horizontal component of velocity/vertical component) was calculated for each bubble analysed in the seven films. Sample histograms for two films taken with and without the probe are shown as figure 6. Both distributions are similar, and it may be concluded that the presence of this probe in the fluidized bed affects neither the overall direction nor the overall shape of the bubbles.

Although the point of the probe was relatively fine there was evidence from some of the photographic studies that a local indentation of the surface was caused in the vicinity of the probe. In addition to the photographic evidence the same conclusion may be drawn from a study of the penetration lengths P_L measured during the simulation of the operation of the probe.

Table 2 shows the average values of the mean penetration lengths and equivalent diameters for the seven films of which one was taken without the probe. One of the principal points of interest in the table is that bubbles in the bed when no probe was present showed a significantly larger penetration although the average bubble diameter was not affected by the presence of the probe. The value of $\overline{P}_L/\overline{D}_e$ when the ratio of major to minor axis was 1.23 is 0.708 from [8] in good agreement with the value of 0.683 given in the table for bubbles when no probe was present. The smaller penetration length and the smaller ratio of $\overline{P}_L/\overline{D}_e$ found when the probe was in position were due to local indentation in the bubble surface caused by the interaction between probe and bubble. The indentation was sufficiently localised so that the overall shape of the bubble was not affected.

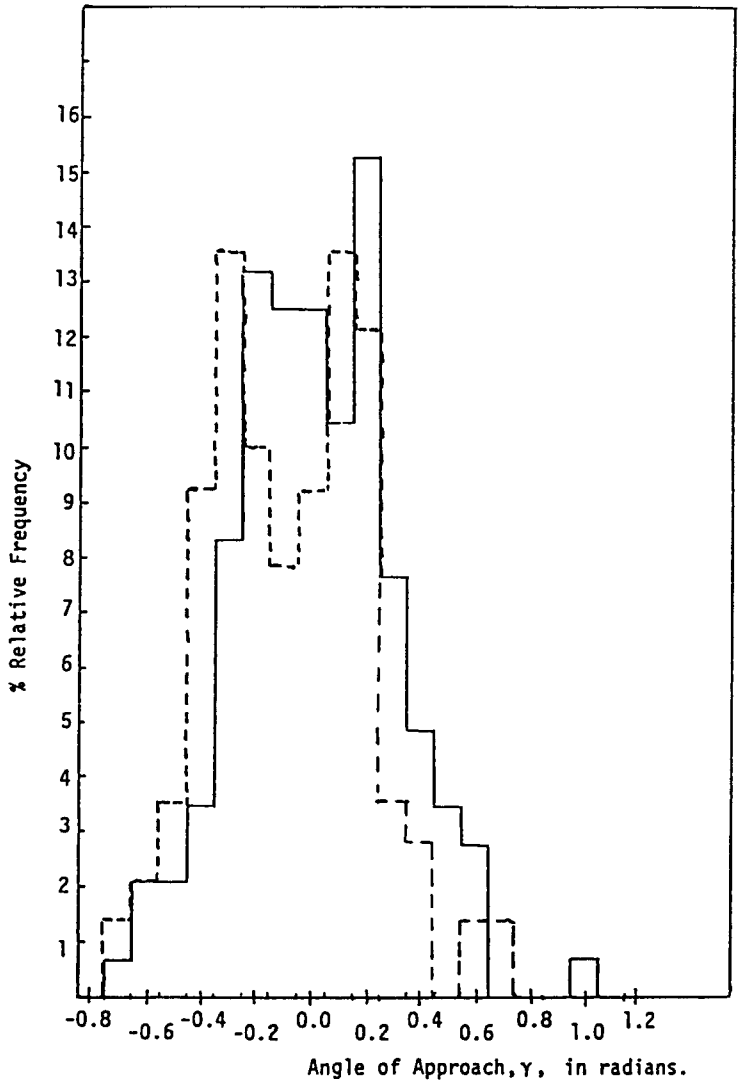

Figure 6. Histogram for distribution of the direction of bubble movement with probe —. Histogram for distribution of the direction of bubble movement without probe ----.

The effect of the probe upon bubble velocity

Table 3 shows the average velocity of the centroid of the bubble, and the average velocity of the upper surface of the bubble measured by the simulation method for each of the seven films.

The elliptical method expresses the vertical rise velocity in terms of the vertical shift of the bubble centroid in the time interval between two successive frames, while the simulation method gives the rise velocity of the upper surface of the bubble. Both velocities show that

Table 2. Penetration lengths and equivalent diameters of bubbles

Film	$\overline{P}_L$ (cm)	$\overline{D}_e$ (cm)	$\overline{P}_L/\overline{D}_e$	State of bed
1	3.18	5.90	0.522	with probe
2	3.26	5.61	0.581	with probe
3	2.81	5.51	0.521	with probe
4	3.56	5.81	0.613	with probe
5	3.27	5.89	0.555	with probe
6	3.20	5.33	0.600	with probe
7	4.03	5.88	0.683	no probe

Table 3. Comparison of bubble velocities

Film no.	Surface velocity mm/s	Centroid velocity mm/s	State of the bed
1	283	312	with probe
2	252	283	with probe
3	230	291	with probe
4	290	301	with probe
5	267	305	with probe
6	300	316	with probe
7	366	356	no probe

bubbles were retarded by the probe, but the retardation experienced by the bubble surfaces contracted by the probe was relatively severe. From table 3 it may be calculated that the mean reduction in surface velocity due to the probe was 26% while the mean reduction of the centroid velocity was 14%.

The corresponding bubble flow rates calculated by [4] for the simulation method and by [6] for the elliptical method are shown in table 4.

It should be made clear that the flowrate obtained by the elliptical method corresponds to the volume of bubbles passing the probe in unit time, so that even though the bubble is retarded, the bubble flowrate is unaffected as [6] shows. The bubble flowrates estimated by the simulation method are lower because as [2], [3] and [4] show, the bubble flowrate is proportional to the penetration length P_L and this quantity is reduced on contact with the probe.

If the bubble flowrate recorded by the simulation method is now multiplied by the ratio of (average penetration length without probe)/(average penetration length with probe) as obtained from table 2, the corrected flowrate shown in table 4 is obtained. The correspondence between the corrected flowrates and the flowrates estimated by the elliptical method is good. The average value of the ratio of penetration lengths from table 2 is 1.25.

The comparison of bubble proportions measured with and without the probe has shown that bubbles are closely elliptical in shape and rise with the major axis horizontal. Bubbles that contact the probe are retarded, and the probe forms an indentation at the point of contact with the leading bubble surface. The indentation causes a reduction in penetration length of 20%, a reduction of 26% in the surface velocity and a reduction of 14% in the centroid velocity. Bubble flowrates obtained by the simulation method, but corrected for the reduction in penetration length showed good agreement with flowrates calculated by the elliptical method.

THE ELECTRICAL RESPONSE OF THE PROBE: THEORY

The optical study of bubbles in the fluidized bed showed that the probes induced deformation in the upper surface of the bubble at the point of impact with the probe. It was also observed that bubbles often showed a significant lateral velocity. Both factors affected

Table 4. Comparison of bubble flowrates measured by the two methods (mm/s)

Film no.	Flowrate by simulation	Flowrate by elliptical method	Corrected flowrate by simulation	State of bed
1	33.2	45.5	43.1	with probe
2	36.6	44.4	45.3	with probe
3	28.6	42.8	40.2	with probe
4	46.8	48.1	53.0	with probe
5	35.8	44.8	44.1	with probe
6	33.8	40.4	43.6	with probe
7	42.5	40.9	42.5	no probe

the response of the probe so that the simpler theory of the photographic simulation of the probe response required modification to describe the electrical response of the probe.

Consider a bubble front of irregular and reentrant shape about to strike the leading probe as shown in figure 7. Because of the influence of lateral velocity and reentrant shape, the vertical rise in the bubble surface X in the time interval of contact between the lower and upper probes will often be less than the separation of the probes h. Define a random variable α such that a line drawn from the upper probe to the impending point of impact of the surface with the upper probe is inclined at an angle α to the vertical as shown in figure 7. The height of rise of the bubble between signals from each probe in the interval Δt_{2i} is

$$x_i = h \cos \alpha_i.$$

If Δt_{1i} is the immersion time of the leading probe in bubble i and Δt_{2i} is the time interval between the bubble front striking the leading and upper probes, the increment of volume sensed by the probe in the effective area of measurement δa is

$$\delta Q_B = \frac{x_i}{\Delta t_{2i}} \Delta t_{1i} \, \delta a \qquad [10]$$

and the total volumetric bubble flow in unit area over a time interval Δt is

$$Q_B = \frac{1}{\Delta t} \sum_{i=1}^{N} \frac{x_i}{\Delta t_{2i}} \Delta t_{1i}. \qquad [11]$$

On substitution for x_i in terms of α_i,

$$Q_B = \frac{h}{\Delta t} \sum_{i=1}^{N} \cos \alpha_i \left[\frac{\Delta t_1}{\Delta t_2}\right]_i. \qquad [12]$$

Suppose that the angle α_i is independent of the ratio $|\Delta t_1/\Delta t_2|_i$ then the average bubble flow will be

$$Q_b = \frac{h}{\Delta t} \sum_{i=1}^{N} \overline{\cos \alpha} \left[\frac{\Delta t_i}{\Delta t_2}\right]_i \qquad [13]$$

and if α_i is symmetrically distributed between the limits of $-\pi/2$ and $\pi/2$,

$$\overline{\cos \alpha} = \frac{2}{\pi} \int_0^{\pi/2} f(\alpha) \cos \alpha \, d\alpha = \phi. \qquad [14]$$

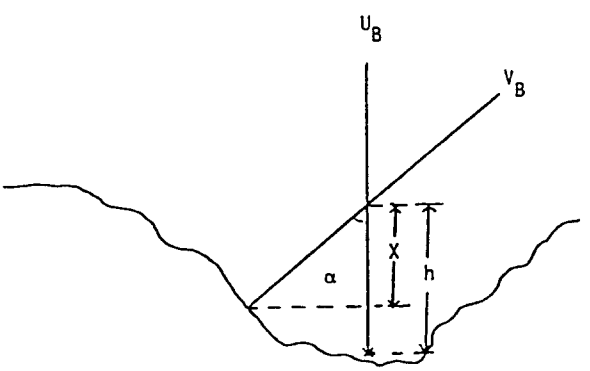

Figure 7. Incidence of bubble surface to probe.

Here $f(\alpha)$ is the probability density so that $f(\alpha)\mathrm{d}\alpha$ is the probability that the angle of inclination lies between α and $\alpha + \mathrm{d}\alpha$.

Thus the volumetric bubble flow through unit area will be

$$Q_B = \frac{\phi h}{t} \sum_{i=1}^{N} \left[\frac{\Delta t_1}{\Delta t_2}\right]_i. \qquad [15]$$

The penetration length P_L defined as the product of the vertical component of the interface velocity U_s and the time of immersion of the leading probe in the bubble is

$$P_L = U_s \Delta t_{1i}$$

$$= \frac{x_i}{\Delta t_{2i}} \Delta t_{1i}$$

so that

$$P_L = h \cos \alpha_i \left[\frac{\Delta t_1}{\Delta t_2}\right]_i. \qquad [16]$$

The average penetration length for N bubbles is

$$\bar{P}_L = \sum_{i=1}^{N} h \cos \alpha_i \left[\frac{t_1}{t_2}\right]_i \Big/ N \qquad [17]$$

and if α_i is taken to be independent of $(\Delta t_1/\Delta t_2)_i$ and the mean is given by [14], the average penetration length is

$$\bar{P}_L = \frac{\phi h}{N} \sum_{i=1}^{N} \left[\frac{\Delta t_1}{\Delta t_2}\right]_i. \qquad [18]$$

COMPARISON OF THE THEORY OF PROBE OPERATION AND EXPERIMENT

As described earlier electrical pulses received for the probes were accepted only if the pulse sequence was valid and if a preset gate voltage in the range to -32 mV was exceeded. The number of bubbles n striking the dual probe was counted from the electronic recording and compared with the number of bubbles N counted from the simultaneous film recording. The ratio of n/N was calculated and is shown in figure 8 as a function of threshold voltage. The value of n/N became very large as the threshold voltage approached zero, and became very small for large threshold voltages so that figure 8 illustrates the feasible working range. A simultaneous film and magnetic probe recording was taken for the gate settings of 12, 17, 21, 25, 28 and 32 mV.

The third method arose from the occurrence of voltage signals that were apparently caused by very fast-moving or slow-moving bubbles that could not be identified in the cine-film recording. The computer program used to process the magnetic tape recording was arranged to accept only bubbles with velocities within the range 0.05 to 2.0 m/s. A record of the rejected bubbles was accumulated by the program. Table 5 shows the proportion of bubbles rejected for each gate setting. It was found that the fraction of sequences rejected was not very sensitive to the precise upper and lower limits. Widening the range to 0.01 to 5.0 m/s, for example, changed the fraction rejected by only a small amount so that an approximate knowledge of the range of velocities only was required.

With the set of internal consistency checks on the integrity of signals arising from the probes, and using the stochastic theory, the mean penetration length, the interface rise

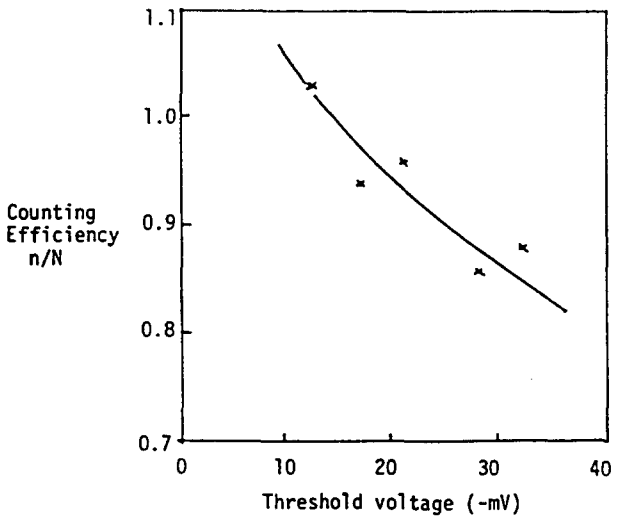

Figure 8. Sensitivity of probe counting to threshold voltage.

velocity and bubble flow may be compared for both the optical and the electrical recordings. The important unknown is the distribution function $f(\alpha)$. In terms of this variable the mean penetration length is given by [18], the bubble flow is given by [13], and the mean interface rise velocity is given by [19],

$$\overline{U}_s = \frac{h}{N}\sum_{i=1}^{N}\frac{\overline{\cos\alpha}}{\Delta t_{2i}}. \qquad [19]$$

If it is supposed that α_i is independent of the time interval Δt_{2i} then the averaged interface velocity becomes

$$\overline{U}_s = \frac{h}{N}\sum_{i=1}^{N}\frac{\overline{\cos\alpha}}{\Delta t_{2i}} = \frac{h}{N}\phi\sum_{i=1}^{N}\frac{1}{\Delta t_{2i}}. \qquad [20]$$

Note however that the statistical independence between α_i and Δt_{2i} is not necessarily the same condition as independence between α_i and the ratio $(\Delta t_{1i}/\Delta t_{2i})$ postulated in obtaining [13] and [18].

A statistical hypothesis both simple and feasible is to suppose that α_i is uniformly distributed in the range $-\pi/2$ to $\pi/2$ so that $\phi = \overline{\cos\alpha} = 2/\pi$ or 0.637. The consistency and truth of this simple hypothesis may be examined by a comparison of electrical and optical recordings of the same bubble flow.

Comparison of mean penetration lengths

The calculation of mean penetration lengths from [18] requires that the value of ϕ (i.e. $\overline{\cos\alpha}$) be known. Alternatively if independent estimates of the mean penetration length are

Table 5. Rejected bubble sequences

Threshold voltage mV	No. of sequences recorded n	No. of sequences discarded		Percentage discarded
		lower limit	upper limit	
−12	140	6	2	5.7
−17	140	4	5	6.4
−21	138	0	3	2.2
−25	135	5	13	13.3
−28	116	8	5	11.2
−32	110	3	14	15.5

Table 6. Values of ϕ from recording and optical simulation of penetration lengths [18]

Threshold voltage mV	P_L mm (optical recording)	$\frac{h}{N}\sum_{i=1}^{N}\left[\frac{\Delta t_1}{\Delta t_2}\right]_i$ mm (electrical recording)	ϕ [18]
−12	31.8	55.3	0.575
−17	32.6	61.3	0.532
−21	28.7	50.6	0.567
−25	35.6	58.9	0.604
−28	32.7	51.8	0.631
−32	32.0	48.7	0.657

available from optical simulation the value of ϕ may be calculated from [18]. Values of mean penetration length from optical simulation are shown in table 2, and values of ϕ calculated from this set are shown in table 6. The number of bubbles examined in each sequence of experiments was approximately 140. The average value of ϕ in the table is 0.594 ± 0.046 standard error but there is a tendency for the value to rise as the threshold voltage becomes more negative.

The expression for ϕ in terms of the probability density $f(\alpha)$ is given by [14]. If the random variable α is uniformly distributed between the limits of $-\pi/2$ and $+\pi/2$ then ϕ is $2/\pi$ or 0.637, i.e. within 7% of the average value above. At low values of threshold voltage the probe response is oversensitive and may count a porosity fluctuation as a bubble, while at high values of threshold voltage the probe response is insensitive and some bubbles may not be counted; as the agreement between $2/\pi$ and the average value is within the standard error of the average value, the simple uniform distribution may be a good approximation to the distribution $f(\alpha)$.

The interface rise velocity

An alternative method of calculating $\phi = \overline{\cos\alpha}$ is from [20] using measurements of the interface rise velocity by optical simulation. The comparison is shown in table 7.

The value of ϕ ($\overline{\cos\alpha}$) when averaged over the table is 0.554 ± 0.067 standard deviation while the value of ϕ when averaged over table 6 is 0.594 ± 0.046 standard deviation, so that the two values agree within the standard deviation of either. However, it is apparent that the value of ϕ in table 6 increases with gate voltage, suggesting that the question of statistical independence is dependent also upon threshold voltage. Hence the evidence of the tables is in support of the hypothesis of statistical independence between both α_i and Δt_{2i}, and α_i and $(\Delta t_{1i}/\Delta t_{2i})$ at the intermediate threshold voltages of tables 6 and 7.

The volumetric bubble flowrate

Equations [18] and [13] show that the bubble flowrate of [13] is based upon the mean penetration length recorded by the probe. The study of the effect of the probe by optical

Table 7. Values of ϕ obtained by recording and optical simulation of interface velocities [20]

Threshold voltage mV	Interface velocity (optical simulation) mm/s	$\frac{h}{N}\sum_{i=1}^{N}\frac{1}{\Delta t_{2i}}$ (electrical recording) mm/s	ϕ [20]
−12	28.3	41.2	0.687
−17	25.2	47.4	0.532
−21	23.0	42.7	0.539
−25	29.0	55.8	0.520
−28	26.7	53.6	0.500
−32	30.0	54.7	0.548

Table 8. Comparison of bubble flowrates from optical simulation and electrical response according to [19]

Threshold voltage mV	Bubble flowrate optical simulation mm/s	Bubble flowrate ϕ table 6 mm/s	Bubble flowrate $\phi = 2/\pi$ mm/s
−12	45.5	41.7	46.1
−17	44.4	39.7	47.5
−21	42.8	37.3	41.9
−25	48.0	40.1	43.1
−28	44.8	33.6	33.9
−32	40.4	32.1	31.1

simulation illustrated in table 4 shows that because of indentations of the bubble by the probe the penetration length is reduced. This may be corrected by multiplying the penetration length by the ratio of (penetration length without probe)/(penetration length with probe), a factor that has been estimated at 1.25. Table 8 shows the volumetric bubble flow rates measured by elliptical simulation (optical) and by two other calculations based upon [18] and [13]. In the first method ϕ is taken from table 6, and in the second method ϕ is taken as $2/\pi$. Thus in both methods the volumetric bubble flowrate is calculated from a combination of [13] and [18] when the factor of 1.25 has been introduced for bubble deformation:

$$Q_B = 1.25 \frac{h}{\Delta t} \phi \sum_{i=1}^{N} \left[\frac{\Delta t_1}{\Delta t_2}\right]_i = 1.25 \frac{N}{\Delta t} \bar{P}_L. \qquad [21]$$

The table clearly shows the similarity of bubble flowrates calculated from each of the three methods except at high values of threshold voltage where bubble flowrates estimated by electrical response are distinctly reduced. Moreover the value of $\phi = 2/\pi$ gives better agreement between electrical response and the optical method. The multiplication of either bubble flowrate by the ratio of total bubbles/bubbles detected by the probe, N/n, did not significantly improve the agreement shown in table 8 except at high threshold voltages so that this additional correction was not made.

CONCLUSION

By a comparison between bubble measurement by optical and electrical methods it has been shown that the measurement of bubble properties by an electrical capacitance probe is feasible. However, it is necessary to select voltage pulses from the capacitance probe so that voltages below a critical threshold are excluded. Thus when the voltage amplitude is −2 V it has been found that the threshold select voltage lies in the range of −12 to −25 mV. For smaller thresholds a sharp increase in estimated bubble flowrate was found because of small voltage signals due to porosity fluctuations; for larger threshold voltages some voltage signals arising from bubbles were excluded so that the recorded bubble flowrate was lower than actual. With the correct threshold voltage set, accurate bubble properties could be measured provided that due allowance was made for the effect of the probe upon the bubble, and provided that an allowance was made for the stochastic interaction between the bubble interface and the probe.

REFERENCES

BAKKER, P. J. 1958 Ph.D. thesis, T. H. Delft.

BURGESS, J. M. & CALDERBANK, P. H. 1975 The measurement of bubble parameters in two-phase dispersions. *Chem. Eng. Sci.* **30**, 743–750, 1511–1518.

CALDERBANK, P. H. & PEREIRA J. 1977 The prediction of distillation plate efficiencies from measured froth properties. 4th Annual Research Meeting I. Chem. E. Swansea.

DAVIES, R. M. & TAYLOR, G. I. 1950 The mechanics of large bubbles rising through extended liquids and through liquids in tubes. *Proc. R. Soc. London Ser. A* **200,** 375–390.

GELDART, D. & KELSEY, J. R. 1972 The use of capacitance probes in gas fluidised beds. *Powder Tech.* **6,** 45–50.

GOLDSCHMIDT, D. & LE GOFF, P. 1967 Electrical methods for the study of a fluidised bed of conducting particles. *Trans. Inst. Chem. E.* **45,** 196–204.

LANNEAU, K. P. 1960 Gas-solids contacting in fluidized beds. *Trans. Inst. Chem. E.* **38,** 125–136.

LOCKETT, M. J. & HARRISON, D. 1967 The distribution of voidage fraction near bubbles rising in gas-fluidized beds. *Proc. Int. Symp. on Fluidization* (Eindhoven), 257–270, Netherlands University Press.

MORSE, R. D. & BALLOU, C. O. 1951 The uniformity of fluidization—its measurement and use. *Chem. Eng. Prog.* **47,** 199–204.

NEAL, L. G. & BANKOFF, S. G. 1963 A high resolution resistivity probe for determination of local void properites in gas–liquid flow. *AIChE. J.* **9,** 490–496.

PARK, W. H., KANG, W. K., CAPES, C. E. & OSBERG, G. L. 1969 The properties of bubbles in fluidized beds of conducting particles as measured by an electro-resistivity probe. *Chem. Eng. Sci.* **24,** 851–865.

ROWE, P. N. & EVERETT, D. J. 1972 Fluidised bed bubbles viewed by X rays. Part II—The transition from two to three dimensions of undisturbed bubbles. *Trans.I.Chem.E.* **50,** 49–54.

ROWE, P. N. & MASSON, H. 1980 Fluidised bed bubbles observed simultaneously by probe and x rays. *Chem. Eng. Sci.* **35,** 1443–1447.

ROWE, P. N. & MASSON, H. 1981 Interaction of bubbles with probes in gas fluidised beds. *Trans. I. Chem. E.* **59,** 177–185.

WERTHER, J. & MOLERUS, O. 1973 The local structure of gas fluidized beds. *Int. Jl. Multiphase Flow* **1,** 103–122.

WERTHER, J. 1974 Bubbles in gas fluidized beds. *Trans. Inst. Chem. E.* **52,** 149–159.

WERTHER, J. 1977 Der Einflüss des Anström bodens auf die Strömungsmechanik von Gas/Feststoff-Wirbelschichten in Euro. Congress on Transfer Processes in Particle Systems, E32–E59, Nuremberg.

WHITEHEAD, A. B. & YOUNG, A. D. 1967 Fluidization Performance in large-scale equipment, Parts I and II. *Proc. Int. Symp. on Fluidization* (Eindhoven), 802–820, Netherlands University Press.

YASUI, G. & JOHANSEN, L. N. 1958 Characteristics of gas pockets in fluidized beds. *AIChE. Jl.* **4,** 445–452.